

Mutual Information Analysis for Factor Graph-based MIMO Iterative Detections through Error Functions

Huan Li, Jingxuan Huang, and Zesong Fei

Abstract

The factor graph (FG) based iterative detection is considered an effective and practical method for multiple-input and multiple-output (MIMO), particularly massive MIMO (m-MIMO) systems. However, the convergence analysis for the FG-based iterative MIMO detection is insufficient, which is of great significance to the performance evaluation and algorithm design of detection methods. This paper investigates the mutual information update flow for the FG-based iterative MIMO detection and proposes a precise mutual information computation mechanism with the aid of Gaussian approximation and error functions, i.e., the error functions-aided analysis (EF-AA) mechanism. Numerical results indicate that the theoretical result calculated by the EF-AA mechanism is completely consistent with the bit error rate performance of the FG-based iterative MIMO detection. Furthermore, the proposed EF-AA mechanism can reveal the exact convergent iteration number and convergent signal-to-ratio value of the FG-based iterative MIMO detection, representing the performance bound of the MIMO detection.

Index Terms

Mutual information, convergence, error functions, Gaussian approximation, MIMO detection, factor graph

I. INTRODUCTION

Ultra-high speed and ultra-reliable wireless transmissions are requested in the sixth-generation (6G) technology to provide ubiquitous high-performance connections [1]. Therefore, multiple-input and multiple-output (MIMO) technology [2] is significant to the 6G implementation, which can guarantee increased data throughput with accurate detection methods. Specifically, massive MIMO (m-MIMO) technology [3] can provide an extremely high data transmission rate due to more transceiver antennas and spatial diversity.

However, most detection algorithms are not feasible for m-MIMO technology because of the inevitable high complexity [4]–[6]. To solve this problem, the authors in [7] proposed to utilize the factor graph (FG) model to transfer probability information between observation nodes (ONs) and variable nodes (VNs) to estimate accurate symbol probabilities. S. Wu et al. in [8] showed that FG-based iterative MIMO detection could achieve near-optimal performance compared to the optimal maximum likelihood detection [4], with a complexity that is acceptable and quadratic to the number of transceiver antennas [9]. Consequently, the FG-based iterative MIMO detection can be considered a practical method for m-MIMO technology.

Specifically, the performance of MIMO detections can be influenced by many factors, for example, the property of MIMO channels. Many prior arts have analyzed the MIMO channel through mutual information [10]–[14]. In [10], O. Oyman et al. derived a tight lower-bounded analytical expression for a Gaussian MIMO frequency-selective spatially correlated fading channel with unknown channel state information (CSI), which approximated the variance of mutual information to a closed-form function. For the space-time independent and identically distributed (i.i.d.) MIMO channel, the authors in [11] proposed

This work has been submitted to the IEEE for possible publication. Copyright may be transferred without notice, after which this version may no longer be accessible.

H. Li, J. Huang and Z. Fei are with the School of Information and Electronics, Beijing Institute of Technology, Beijing 100081, China (e-mail: huan_lilh@outlook.com and 3120200780@bit.edu.cn, jxhbit@gmail.com, feizesong@bit.edu.cn.).

analytical expressions to present the distribution characters of mutual information between transmitted and received signal vectors. L. Musavian et al. proved in [12] that a tight gap between the upper and lower bounds of mutual information exists when uncorrelated transmit antennas with uniform power distribution and correlated receive antennas are considered. For the m-MIMO systems, P. Yang et al. have developed a message-passing-based algorithm to compute the mutual information where arranged finite-alphabet inputs [13]. Recently, random matrix theory has been utilized to attain the ergodic mutual information between the transmit signals and outputs of the Rayleigh channel [14], which is quantized by a mixed analog-to-digital converters architecture.

Based on the mutual information investigations of different MIMO channels, much literature has studied the performance of varieties of MIMO detections from the perspective of mutual information. For the serial detection schemes in vertical Bell labs layered space-time (V-BLAST) MIMO architecture [15], S. Stiglmayr et al. calculated the mutual information of a single antenna stream without considering the correlation between the Gaussian noise and hard decision error [16]. In [17], the authors proposed a numerical calculation of the mutual information to show the convergence of an iterative method, which utilized the stair matrix to achieve similar performance to linear minimum mean-square error (MMSE) detection. Particularly for the belief propagation-based iterative detections, [18] employed the extrinsic information transfer (EXIT) chart to present the validity and convergence of the iterative process. Then, we initially derived the closed-form mutual information update flow for the FG-based iterative MIMO detection according to the EXIT analysis in [19]. Nevertheless, the proposed mutual information calculations in [19] ignored the specific probability when computing the mutual information between VN and the transmitted symbol. The existing approximation of mutual information causes inaccuracy in evaluating the convergence and bit error rate (BER) performance.

Therefore, we derive the closed-form expressions of assessing the convergence and BER performance of the FG-based iterative MIMO detection, which is more feasible for the MIMO, especially the m-MIMO system. In this paper, we proposed a more precise calculation method for the mutual information update flow of the FG-based iterative MIMO detection under both binary phase shift keying (BPSK) and quadrature phase shift keying (QPSK) modulations, where the error function $erf(\cdot)$ and the complementary error function $erfc(\cdot)$ are utilized. Our proposed error functions-aided mechanism can provide exact mutual information curves at different SNRs in both MIMO and m-MIMO systems, which are of great significance to theoretical bound evaluation and the detection algorithm designs.

Noted that this work is distinct from the aforementioned studies [10]–[14], which focuses on precisely investigating the performance of FG-based iterative MIMO detections, instead of MIMO channel properties. The rest of this paper is organized as follows. In Section II, the system model and fundamental knowledge of FG-based iterative MIMO detections are introduced. In Section III, we derived the proposed error functions-aided mutual information calculation mechanism for FG-based iterative MIMO detections. The numerical results of mutual information analysis and the BER performance are presented in Section IV. Finally, we conclude this paper in Section V.

II. PRELIMINARIES

A. Channel Model

In this paper, we consider a MIMO system equipped with numerous antennas at both the transmit and receive sides, represented by N_T and N_R , respectively. Note that the number of antennas can range from 2 to hundreds. Specifically, the received signal vector $\mathbf{y} \in \mathbb{C}^{N_R \times 1}$ can be given as

$$\mathbf{y} = \mathbf{H}\mathbf{x} + \mathbf{n}, \quad (1)$$

where $\mathbf{x} = [x_1, x_2, \dots, x_{N_T}] \in \mathbb{C}^{N_T \times 1}$ denotes the power-normalized transmitted signal vector, $\mathbf{n} = [n_1, n_2, \dots, n_{N_R}] \in \mathbb{C}^{N_R \times 1}$ denotes the additive complex-valued Gaussian white noise, which can be

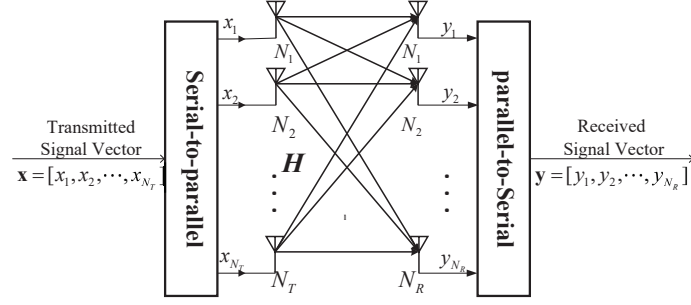


Fig. 1. V-BLAST architecture.

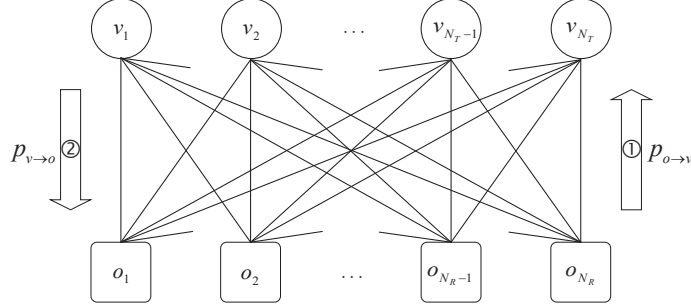


Fig. 2. Information transfer flow in FG-based iterative MIMO detections.

represented as $n_i \sim \mathcal{CN}(0, \sigma_n^2)$. The channel matrix $\mathbf{H} \in \mathbb{C}^{N_R \times N_T}$ reflects the Rayleigh fading effects and can be expressed as

$$\mathbf{H} = \begin{bmatrix} h_{1,1} & \cdots & h_{1,N_T} \\ \vdots & \ddots & \vdots \\ h_{N_R,1} & \cdots & h_{N_R,N_T} \end{bmatrix}, \quad (2)$$

where entries follow the complex-valued Gaussian distribution with zero mean and unit variance.

Specifically, the V-BLAST MIMO structure [15] is adopted at the transmit and receive sides, shown as Fig. 1. To evaluate the performance of FG-based iterative MIMO detections more precisely, the averaged received SNR ρ_r is given as

$$\rho_r = \mathbb{E} \left\{ \frac{\sum_{i=1, j=1}^{i=N_R, j=N_T} |h_{i,j}|^2}{N_T \sigma_n^2} \right\}. \quad (3)$$

B. An Overview of the FG-based Iterative MIMO Detection

The FG-based MIMO detection is a kind of message-passing algorithm, which transmits *a posteriori* probability information between ONs o_i ($i = 1, 2, \dots, N_R$) and VNs v_l ($l = 1, 2, \dots, N_T$). The specific information transfer flow in FG is given in Fig. 2.

Shown as in Fig. 2, the FG-based iterative MIMO detection firstly transmit the probability information $p_{o \rightarrow v}$ from ON to VN, which is given as

$$p_{o \rightarrow v} = \prod_{v' \in V(o) \setminus v} p_{v' \rightarrow o}, \quad (4)$$

where $V(o) \setminus v$ denotes the collection of VN connected to ON except VN v .

Then the probability information $p_{v \rightarrow o}$ transferred from VN to ON can be expressed as

$$p_{v \rightarrow o} = \prod_{o' \in O(v) \setminus o} p_{o' \rightarrow v}, \quad (5)$$

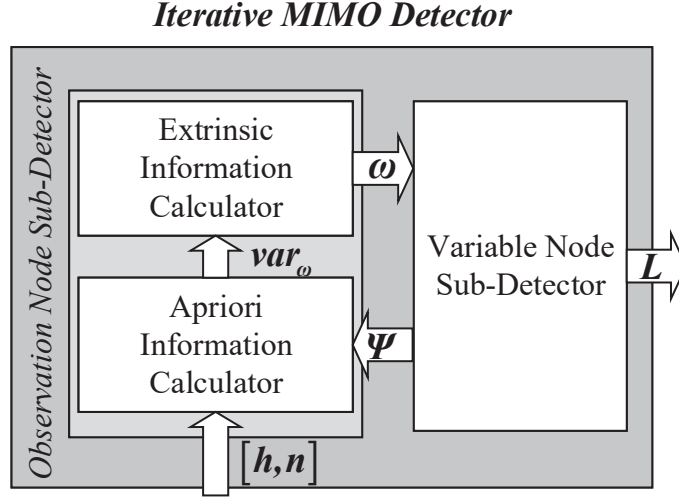


Fig. 3. Extrinsic information transfer flow for iterative MIMO detections.

where $O(v) \setminus o$ represents the collection of ON linked to VN except ON o .

To conclude, the FG-based iterative MIMO detection follows the bidirectional-transmission mechanism until the *a posteriori* probability information stays unchanged, which is defined as convergence [20].

III. ERROR FUNCTIONS-AIDED ANALYSIS MECHANISM FOR FG-BASED ITERATIVE MIMO DETECTIONS

In our previous work [19], we introduced an innovative EXIT analysis method with the ability to evaluate mutual information through low-complexity calculations. Although the earlier EXIT analysis was able to present the convergence of iterative MIMO detections, it was not accurate enough. In this paper, we propose a new method that can generate mutual information curves of iterative MIMO detections more precisely.

The information transfer flow of FG-based iterative MIMO detections can be demonstrated in Fig. 3, where the iterative MIMO detector is abstracted to be composed of the ON sub-detector and VN sub-detector. Specifically, the ON sub-detector concludes two components, i.e., the extrinsic information calculator (EIC) and the apriori information calculator (AIC).

As shown in Fig. 3, the AIC firstly updates the information transferred to it, utilizing channel information $h_{i,l}$, n_i ($i = 1, 2, \dots, N_R$, $l = 1, 2, \dots, N_T$) transformed by VN sub-detector. Hence, the output information $var_{\omega_i^l}$ of AIC can be expressed as

$$\begin{aligned} var_{\omega_i^l} &= F_{AIC}(c_{i,l}, \psi_i^l), \\ \text{for } i &= 1, 2, \dots, N_R, \text{ and } j = 1, 2, \dots, N_T, \end{aligned} \quad (6)$$

where $F_{AIC}(\cdot)$ denotes the transfer function of AIC.

Another component of the ON sub-detector is EIC, which calculates the mutual information $I_{\omega_i^l}$ between transmit symbol x_l and LLR ω_i^l , and then transfer the mutual information $I_{\omega_i^l}$ to VN sub-detector. The mutual information $I_{\omega_i^l}$ can be represented by (7), where $p_{\omega}(\omega_i^l|x_l)$ denotes the conditional probability density function (CPDF) of the LLR ω_i^l at ON o_i . In addition, $F_{\omega}(\cdot)$ denotes the transfer function of VN-detector, which also indicates that the CPDF $p_{\omega}(\omega_i^l|x_l)$ is relevant to the output information of AIC $var_{\omega_i^l}$.

For the VN sub-detector, mutual information $I_{\psi_i^l}$ between transmit symbol x_l and LLR ψ_i^l is related to the output information of EIC ω_i^l , and can be expressed by 8, which is then transferred to ON sub-detector. In (8), $p_{\psi}(\psi_i^l|x_l)$ represents the CPDF of the LLR ψ_i^l at VN v_l . Similarly, $F_{\psi}(\cdot)$ denotes the

$$I_{\omega_i^l} = I(x_l; \omega_i^l) \triangleq \frac{1}{2} \sum_{\theta=\theta_1, \theta_2} \int_{-\infty}^{+\infty} p_{\omega}(\omega_i^l | x_l = \theta) \log_2 \left(\frac{2p_{\omega}(\omega_i^l | x_l = \theta)}{p_{\omega}(\omega_i^l | x_l = \theta_1) + p_{\omega}(\omega_i^l | x_l = \theta_2)} \right) d\omega_i^l \quad (7)$$

$$\triangleq F_{\omega} \left(var_{\omega_i^l} \right),$$

$$I_{\psi_i^l} = I(x_l; \psi_i^l) \triangleq \frac{1}{2} \sum_{\theta=\theta_1, \theta_2} \int_{-\infty}^{+\infty} p_{\psi}(\psi_i^l | x_l = \theta) \log_2 \left(\frac{2p_{\psi}(\psi_i^l | x_l = \theta)}{p_{\psi}(\psi_i^l | x_l = \theta_1) + p_{\psi}(\psi_i^l | x_l = \theta_2)} \right) d\psi_i^l \quad (8)$$

$$\triangleq F_{\psi} \left(var_{\psi_i^l} \right),$$

transfer function of VN sub-detector, and the CPDF $p_{\psi}(\psi_i^l | x_l)$ is related to the output information of EIC ω_i^l . Furthermore, the output information $L_l = \sum_{i'=1}^{N_R} \omega_{i'}^l$ of the iterative MIMO detection is also relevant to the output information of EIC ω_i^l , then the mutual information of which can be given as

$$I_{L_l} = F_L \left(var_{\omega_i^l} \right), \quad (9)$$

where $F_L(\cdot)$ represents the transfer function of iterative MIMO detector.

A. The Error Functions-Aided Analysis under BPSK Modulation

This paper first derives the analysis mechanism for FG-based iterative MIMO detections under BPSK modulation. The previous work [19] has derived the approximate mutual information of the ON sub-detector and VN sub-detector. Although the analysis in [19] is imperfect, it still provides some significant derivation for our current work, which are concluded as **Lemma 1** to **Lemma 3** as follows.

Lemma 1 The mutual information $I_{\omega_i^l}$ between transmitted symbol x_l and LLR ω_i^l at ON o_i can be expressed as

$$I_{\omega_i^l} \triangleq F_{\omega} \left(var_{\omega_i^l} \right) \triangleq J(\sqrt{var_{\omega_i^l}}), \quad (10)$$

where $J(\cdot)$ is a curve fitting function for the integral in (7) proposed in [21], which is given in Appendix A.

Specifically, $var_{\omega_i^l}$ was defined as the equivalent channel variable (ECV) [19] transferred by the AIC, which is computed based on the channel information integrated with extrinsic information from VN sub-detector as follows

$$var_{\omega_i^l} = \frac{4h_{i,l}^2}{\sigma_{g_{il}}^2}, \quad (11)$$

where $\sigma_{g_{il}}^2$ denotes the variance of interference signals (i.e., signals from other antennas sum up with channel noise).

The details can be seen in [19].

Lemma 2 The CPDF of extrinsic LLR ψ_i^l at VN v_l follows the Gaussian distribution of mean $\mu_{\psi_i^l}$ and variance $var_{\psi_i^l}$, which can be represented as

$$p_{\psi}(\psi_i^l | x_l) = p_{\psi}(\psi_i^l | h_{i,l}, x_l)$$

$$= \frac{1}{\sqrt{2\pi var_{\psi_i^l}}} \exp \left(-\frac{(\psi_i^l - \mu_{\psi_i^l})^2}{2var_{\psi_i^l}} \right), \quad (12)$$

where $var_{\psi_i^l}$ denotes the variance of the extrinsic LLR ψ_i^l , and can be calculated by

$$\begin{aligned} var_{\psi_i^l} &= \sum_{i'=1, i' \neq i}^{N_R} var_{\omega_{i'}^l} \\ &= \sum_{i'=1, i' \neq i}^{N_R} J^{-1} \left(I_{\omega_{i'}^l} \right), \end{aligned} \quad (13)$$

where $J^{-1}(\cdot)$ denotes the inverse function of the curve fitting function $J(\cdot)$, which is given in Appendix A. Furthermore, the mean value is given as

$$\begin{aligned} \mu_{\psi_i^l} &= \pm \frac{var_{\psi_i^l}}{2} \\ &= \sum_{i'=1, i' \neq i}^{N_R} \pm \frac{var_{\omega_{i'}^l}}{2}. \end{aligned} \quad (14)$$

The details can be seen in [19].

Lemma 3 The mutual information $I_{\psi_i^l}$ between transmitted symbol x_l and LLR ψ_i^l at VN v_l is given as

$$I_{\psi_i^l} \triangleq F_{\psi} \left(var_{\psi_i^l} \right) = J \left(\sqrt{var_{\psi_i^l}} \right). \quad (15)$$

The details can be seen in [19].

In what follows, we derive the mutual information $I_{\omega_i^l}$, $I_{\psi_i^l}$ and I_{L_l} according to Fig. 3 and the aforementioned **Lemmas**, respectively. It is noted that the mutual information $I_{\omega_i^l}$ calculated by EIC at ON sub-detector is given in **Lemma 1** as (10), with parameter $var_{\omega_i^l}$ as the input. Furthermore, the mutual information $I_{\psi_i^l}$ computed at VN sub-detector is defined in **Lemma 3** as (15), and the input parameter $var_{\psi_i^l}$ can be obtained through the summation of $var_{\omega_i^l}$. Therefore, in this section, we mainly focus on the computation of the variance $var_{\omega_i^l}$ at the AIC, i.e., the function $F_{AIC}(\cdot)$ in (6).

At AIC, the received symbol y_i can be separated into two parts, namely the symbol from the corresponding transmit antenna and interference, which is given as

$$\begin{aligned} y_i &= \sum_{l=1}^{N_T} h_{i,l} x_l + n_i \\ &= h_{i,l} x_l + \underbrace{\sum_{l'=1, l' \neq l}^{N_T} h_{i,l'} x_{l'}}_{g_{il}} + n_i, \end{aligned} \quad (16)$$

where the signals from other antennas plus channel noise are approximated to Gaussian random variables as $g_{il} \sim \mathcal{N}(\mu_{g_{il}}, \sigma_{g_{il}}^2)$. Specifically, the mean $\mu_{g_{il}}$ and variance $\sigma_{g_{il}}^2$ can be computed as

$$\mu_{g_{il}} = \sum_{l'=1, l' \neq l}^{N_T} h_{i,l'} \mathbb{E}(x_{l'}), \quad (17)$$

$$\sigma_{g_{il}}^2 = \sum_{l'=1, l' \neq l}^{N_T} |h_{i,l'}|^2 \mathbb{V}(x_{l'}) + \sigma_n^2, \quad (18)$$

in which

$$\mathbb{E}(x_{l'}) = \sum_{j=1}^2 P_i^{l'}(\theta_j) \cdot \theta_j, \quad (19)$$

and

$$\mathbb{V}(x_{l'}) = \sum_{j=1}^2 P_i^{l'}(\theta_j) \cdot \theta_j^2 - |\mathbb{E}(x_{l'})|^2, \quad (20)$$

are the mean and variance of $x_{l'}$ respectively, in which $P_i^{l'}(\theta_j)$ represents the probability of $x_{l'} = \theta_j \in \{\pm 1\}$ estimated at VN $v_{l'}$.

From **Lemma 1**, we get to know that the ECV $var_{\omega_i^l}$ is essential to the calculation of mutual information I_{ω} . Formula (11) also indicates that the critical part of ECV $var_{\omega_i^l}$ is the variance $\sigma_{g_{il}}$. Furthermore,

according to (18) and (20), the calculation of probability $P_i^l(\theta_j)$ at VN v_l is indispensable for the computation of variance $\sigma_{g_{il}}$, as well as the ECV $var_{\omega_i^l}$.

Specifically, the $P_i^l(\theta_j)$ at VN v_l can be initialized as an equal probability in the first iteration during the iterative MIMO detections. Therefore, in the first iteration, we have

$$\begin{aligned} \mathbb{V}(x_l) &= \frac{1}{2} (1^2 + (-1)^2) - \left| \frac{1}{2} (1 - 1) \right|^2 \\ &= 1. \end{aligned} \quad (21)$$

However, the variance $\mathbb{V}(x_l)$ remains uncertain in the subsequent iterations, for the reason that $P_i^l(\theta_j)$ is changeable with the LLR ω_i^l transferred from the ON sub-detector. Consequently, it is crucial to derive the probability $P_i^l(\theta_j)$ at VN v_l in the subsequent iterations. Before that, we propose the following **Theorem 1** as the basis of our further analysis.

Theorem 1 Given the PDF $p_L(L_\alpha)$ of LLR L_α for symbol α , we can get the probability of symbol $\alpha = 1$ as

$$P(\alpha = 1) = \int_0^\infty p_L(L_\alpha) dL_\alpha. \quad (22)$$

Similarly, the probability of symbol $\alpha = 0$ is given as

$$P(\alpha = 0) = \int_{-\infty}^0 p_L(L_\alpha) dL_\alpha. \quad (23)$$

Proof: In the process of iterative MIMO detection, hard decision adopts the following criteria

$$\alpha = \begin{cases} 1, & \text{if } L_\alpha > 0 \\ 0, & \text{if } L_\alpha < 0 \end{cases}, \quad (24)$$

which indicates the value of α depends on the sign of its LLR L_α . While given the probability of the symbol's LLR, instead of its accurate value, we can only obtain the probability of $P(L_\alpha > 0)$ and $P(L_\alpha < 0)$ through the integral of $p_L(L_\alpha)$, which can be expressed as

$$P(L_\alpha > 0) = \int_0^\infty p_L(L_\alpha) dL_\alpha, \quad (25)$$

and

$$P(L_\alpha < 0) = \int_{-\infty}^0 p_L(L_\alpha) dL_\alpha. \quad (26)$$

Thus, combined with (25) and (26), which reflect the sign of L_α through probability, (24) can be revised as

$$\begin{cases} P(\alpha = 1) \propto P(L_\alpha > 0) \\ P(\alpha = 0) \propto P(L_\alpha < 0) \end{cases}. \quad (27)$$

Therefore, we can represent the probability of α as (22) and (23), respectively. ■

In **Lemma 2**, the CPDF of extrinsic LLR ψ_i^l at VN v_l is given as a Gaussian PDF with known mean and variance. Then we can derive the probability $P_i^l(\theta_j)$ at VN v_l in the subsequent iterations according to **Theorem 1** and the CPDF (12) in **Lemma 2**.

Theorem 2 Given the variance $var_{\psi_i^l}$ of extrinsic LLR ψ_i^l of VN sub-detector, we can calculate the probability $P_i^l(\theta_j)$ estimated at VN v_l in the subsequent iterations as follows

$$\begin{aligned} P_i^l(+1) &= P_i^l(\theta_j = +1) \\ &= \begin{cases} \frac{1}{2} \left[1 + \operatorname{erf} \left(\sqrt{\frac{var_{\psi_i^l}}{8}} \right) \right], & \text{if } x_l = +1, \\ \frac{1}{2} \operatorname{erfc} \left(\sqrt{\frac{var_{\psi_i^l}}{8}} \right), & \text{if } x_l = -1, \end{cases} \end{aligned} \quad (28)$$

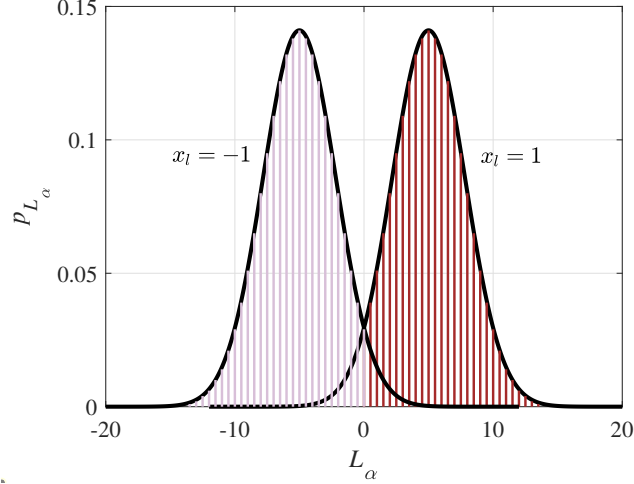


Fig. 4. The probability of right-decision $P_i^l(\theta_j \rightarrow R)$ represented by the integral of $p_\psi(\psi_i^l|x_l = \mp 1)$ (see the shadowing parts).

and

$$\begin{aligned} P_i^l(-1) &= P_i^l(\theta_j = -1) \\ &= \begin{cases} \frac{1}{2} \left[1 + \operatorname{erf} \left(\sqrt{\operatorname{var}_{\psi_i^l}/8} \right) \right], & \text{if } x_l = -1, \\ \frac{1}{2} \operatorname{erfc} \left(\sqrt{\operatorname{var}_{\psi_i^l}/8} \right), & \text{if } x_l = +1, \end{cases} \end{aligned} \quad (29)$$

where $\operatorname{erf}(\cdot)$ and $\operatorname{erfc}(\cdot)$ are the error function and complementary error function respectively, which were defined in [22] as

$$\operatorname{erf}(x) = \frac{2}{\sqrt{\pi}} \int_0^x \exp(-t^2) dt, \quad (30)$$

and

$$\operatorname{erfc}(x) = 1 - \operatorname{erf}(x) = \frac{2}{\sqrt{\pi}} \int_x^\infty \exp(-t^2) dt. \quad (31)$$

Proof: From aforementioned **Lemma 2** we can know that the CPDF estimated at VNs follows the Gaussian distribution, and is given as

$$\begin{aligned} p_\psi(\psi_i^l|h_{i,l}, x_l) &= p_\psi(\psi_i^l|x_l = \mp 1) \\ &= \frac{1}{\sqrt{2\pi \operatorname{var}_{\psi_i^l}}} \exp \left(-\frac{\left(\psi_i^l \pm \operatorname{var}_{\psi_i^l}/2 \right)^2}{2\operatorname{var}_{\psi_i^l}} \right), \end{aligned} \quad (32)$$

which is determined by the transmit symbol x_l .

Combined with **Theorem 1**, we define the probability of right-decision $P_i^l(\theta_j \rightarrow R)$ and wrong-decision $P_i^l(\theta_j \rightarrow W)$ at VNs. The corresponding shadowing parts in Fig. 4 and Fig. 5 are presented to better illustrate $P_i^l(\theta_j \rightarrow R)$ and $P_i^l(\theta_j \rightarrow W)$, respectively. Then The calculation of $P_i^l(\theta_j \rightarrow R)$ and $P_i^l(\theta_j \rightarrow W)$ are derived as (33) and (34). It is noted that the detailed deduction of (33.a) and (34.a) is shown in Appendix B.

Hence, we can conclude the probability $P_i^l(\theta_j)$ estimated at VN v_l as (28) and (29), which discuss the probability $P_i^l(\theta_j)$ based on $P_i^l(\theta_j \rightarrow R)$ and $P_i^l(\theta_j \rightarrow W)$, as well as the uncertain transmit symbol $x_l = \mp 1$. ■

Theorem 2 presents the expression of probability $P_i^l(\theta_j)$, based on which we can further deduct the ECV $\operatorname{var}_{\omega_i^l}$ calculated at AIC.

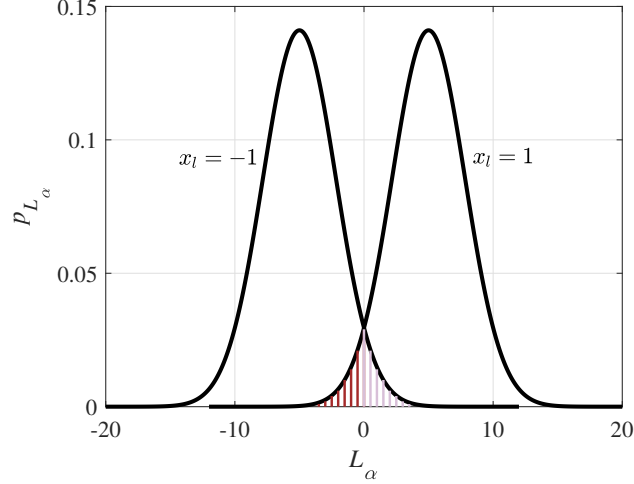


Fig. 5. The probability of wrong-decision $P_i^l(\theta_j \rightarrow W)$ represented by the integral of $p_\psi(\psi_i^l | x_l = \mp 1)$ (see the shadowing parts).

$$\begin{aligned}
P_i^l(\theta_j \rightarrow R) &= \sum_{x_l = \theta_j} P(x_l) P(\theta_j | x_l) \\
&= \frac{1}{2} \int_0^\infty p_\psi(\psi_i^l | x_l = \theta_j = 1) d\psi_i^l + \frac{1}{2} \int_{-\infty}^0 p_\psi(\psi_i^l | x_l = \theta_j = -1) d\psi_i^l \\
&\stackrel{(a)}{=} \frac{1}{2\sqrt{2\pi \text{var}_{\psi_i^l}}} \left\{ \int_0^\infty \exp\left(-\frac{(\psi_i^l - \text{var}_{\psi_i^l}/2)^2}{2\text{var}_{\psi_i^l}}\right) d\psi_i^l + \int_{-\infty}^0 \exp\left(-\frac{(\psi_i^l + \text{var}_{\psi_i^l}/2)^2}{2\text{var}_{\psi_i^l}}\right) d\psi_i^l \right\} \\
&\stackrel{(b)}{=} \frac{1}{4} \left[1 + \text{erf}\left(\sqrt{\frac{\text{var}_{\psi_i^l}}{8}}\right) \right] + \frac{1}{4} \left[1 + \text{erf}\left(\sqrt{\frac{\text{var}_{\psi_i^l}}{8}}\right) \right] \\
&= \frac{1}{2} \left[1 + \text{erf}\left(\sqrt{\frac{\text{var}_{\psi_i^l}}{8}}\right) \right].
\end{aligned} \tag{33}$$

Theorem 3 According to (11) in **Lemma 1**, the ECV $\text{var}_{\omega_i^l}$ calculated at AIC can be calculated as

$$\text{var}_{\omega_i^l} = \frac{2h_{i,l}^2}{\sum_{l'=1, l' \neq l}^{N_T} |h_{i,l'}|^2 \mathbb{V}(x_{l'}) + \sigma_n^2}, \tag{35}$$

where

$$\mathbb{V}(x_l) = \begin{cases} 1, & t = 1, \\ \left[1 + \text{erf}\left(\sqrt{\frac{\text{var}_{\psi_i^l}}{8}}\right) \right] \text{erfc}\left(\sqrt{\frac{\text{var}_{\psi_i^l}}{8}}\right), & t > 1, \end{cases} \tag{36}$$

in which the first line is calculated according to the first-iteration variance $\mathbb{V}(x_l)$ in (21), and t denotes the iteration times during the MIMO detection.

Proof: The variance $\mathbb{V}(x_l)$ in the first iteration is calculated as in (21), thus we mainly derive $\mathbb{V}(x_l)$ when $t > 1$ in this theorem.

based on **Theorem 2** and **Lemma 1** we discuss the ECV $\text{var}_{\omega_i^l}$ calculated at AIC on two cases, i.e., the transmit symbol $x_l = 1$ and $x_l = -1$. The specific derivation is shown as follows:

$$\begin{aligned}
P_i^l(\theta_j \rightarrow W) &= \sum_{x_l \neq \theta_j} P(x_l)P(\theta_j|x_l) \\
&= \frac{1}{2} \int_0^\infty p_\psi(\psi_i^l|x_l = -\theta_j = -1)d\psi_i^l + \frac{1}{2} \int_{-\infty}^0 p_\psi(\psi_i^l|x_l = -\theta_j = 1)d\psi_i^l \\
&\stackrel{(a)}{=} \frac{1}{2\sqrt{2\pi\text{var}_{\psi_i^l}}} \left\{ \int_0^\infty \exp\left(-\frac{(\psi_i^l + \text{var}_{\psi_i^l}/2)^2}{2\text{var}_{\psi_i^l}}\right) d\psi_i^l + \int_{-\infty}^0 \exp\left(-\frac{(\psi_i^l - \text{var}_{\psi_i^l}/2)^2}{2\text{var}_{\psi_i^l}}\right) d\psi_i^l \right\} \\
&\stackrel{(b)}{=} \frac{1}{4} \left[\text{erfc}\left(\sqrt{\frac{\text{var}_{\psi_i^l}}{8}}\right) \right] + \frac{1}{4} \left[\text{erfc}\left(\sqrt{\frac{\text{var}_{\psi_i^l}}{8}}\right) \right] \\
&= \frac{1}{2} \text{erfc}\left(\sqrt{\frac{\text{var}_{\psi_i^l}}{8}}\right).
\end{aligned} \tag{34}$$

C1: The transmit symbol $x_l = 1$. With the probabilities $P_i^l(+1)$ estimated at VN v_l shown as (28) and (29), we can obtain the mean value $\mathbb{E}(x_{l+}^+)$ of x_l according to (19) as

$$\begin{aligned}
\mathbb{E}(x_{l+}^+) &= \frac{+1}{2} \left[1 + \text{erf}\left(\sqrt{\frac{\text{var}_{\psi_i^l}}{8}}\right) \right] - \frac{1}{2} \text{erfc}\left(\sqrt{\frac{\text{var}_{\psi_i^l}}{8}}\right) \\
&= \text{erf}\left(\sqrt{\frac{\text{var}_{\psi_i^l}}{8}}\right).
\end{aligned} \tag{37}$$

Then based on (20), the variance $\mathbb{V}(x_{l+}^+)$ of x_l can be given as

$$\begin{aligned}
\mathbb{V}(x_{l+}^+) &= (1)^2 P_i^l(1) + (-1)^2 P_i^l(-1) - |\mathbb{E}(x_l)|^2 \\
&= [P_i^l(1) + P_i^l(-1)] - \left[\text{erf}\left(\sqrt{\frac{\text{var}_{\psi_i^l}}{8}}\right) \right]^2 \\
&= 1 - \text{erf}\left(\sqrt{\frac{\text{var}_{\psi_i^l}}{8}}\right)^2 \\
&= \left[1 + \text{erf}\left(\sqrt{\frac{\text{var}_{\psi_i^l}}{8}}\right) \right] \left[1 - \text{erf}\left(\sqrt{\frac{\text{var}_{\psi_i^l}}{8}}\right) \right] \\
&= \left[1 + \text{erf}\left(\sqrt{\frac{\text{var}_{\psi_i^l}}{8}}\right) \right] \text{erfc}\left(\sqrt{\frac{\text{var}_{\psi_i^l}}{8}}\right).
\end{aligned} \tag{38}$$

C2: The transmit symbol $x_l = -1$. With the probabilities $P_i^l(\mp 1)$ estimated at VN v_l shown as (28) and

(29), we can obtain the mean value $\mathbb{E}(x_l^-)$ of x_l according to (19) as

$$\begin{aligned}\mathbb{E}(x_l^-) &= \frac{-1}{2} \left[1 + \operatorname{erf} \left(\sqrt{\frac{\operatorname{var}_{\psi_i^l}}{8}} \right) \right] + \frac{1}{2} \operatorname{erfc} \left(\sqrt{\frac{\operatorname{var}_{\psi_i^l}}{8}} \right) \\ &= \frac{1}{2} \left[\operatorname{erfc} \left(\sqrt{\frac{\operatorname{var}_{\psi_i^l}}{8}} \right) - \operatorname{erf} \left(\sqrt{\frac{\operatorname{var}_{\psi_i^l}}{8}} \right) - 1 \right] \\ &= -\operatorname{erf} \left(\sqrt{\frac{\operatorname{var}_{\psi_i^l}}{8}} \right).\end{aligned}\quad (39)$$

Similarly, the variance $\mathbb{V}(x_l^-)$ of x_l is expressed as

$$\begin{aligned}\mathbb{V}(x_l^-) &= 1 - \left[\operatorname{erf} \left(\sqrt{\frac{\operatorname{var}_{\psi_i^l}}{8}} \right) \right]^2 \\ &= \left[1 + \operatorname{erf} \left(\sqrt{\frac{\operatorname{var}_{\psi_i^l}}{8}} \right) \right] \operatorname{erfc} \left(\sqrt{\frac{\operatorname{var}_{\psi_i^l}}{8}} \right).\end{aligned}\quad (40)$$

which is identical to (38).

Therefore, we can conclude that the variance $\mathbb{V}(x_l)$ is unrelated to the value of transmit symbol x_l , and can be represented identically as (36). Then substitute (36) into (18) and (11), we can acquire this theorem. \blacksquare

Consequently, given the variance $\operatorname{var}_{\omega_i^l}$ at AIC as (35) and (36) in **Theorem 3**, the mutual information $I_{\omega_i^l}$ can be calculated according to (10) at the EIC (i.e., ON sub-detector). Then the mutual information $I_{\psi_i^l}$ at the VN sub-detector can be computed as (15). In addition, the mutual information I_{L_l} between the LLR L_l output by the VN sub-detector and transmit symbol x_l is given as

$$I_{L_l} \triangleq F_L \left(\operatorname{var}_{\omega_i^l} \right) = J \left(\sqrt{\sum_{i'=1}^{N_R} \operatorname{var}_{\omega_{i'}^l}} \right), \quad (41)$$

then the averaged mutual information (AMI) of the VNs I_L can be expressed as

$$I_L = \frac{1}{N_T} \sum_{l=1}^{N_T} I_{L_l}. \quad (42)$$

To sum up, the error functions-aided analysis (EF-AA) mechanism for FG-based iterative MIMO detections under the BPSK modulation can be summarized as Algorithm 1.

B. The Error Functions-Aided Analysis under QPSK Modulation

According to [23], the complex-domain Rayleigh fading MIMO channel (2) can be converted into an equivalent real-domain form, which extracts the real and imaginary part of each entry in (2), respectively. The conversion can be presented by

$$\mathbf{H}_R = \begin{bmatrix} \Re(\mathbf{H}) & -\Im(\mathbf{H}) \\ \Im(\mathbf{H}) & -\Re(\mathbf{H}) \end{bmatrix}, \quad (43)$$

where $\Re(\cdot)$ and $\Im(\cdot)$ denote the real part and imaginary part of elements, respectively. Then the corresponding vectors in (2) can be transformed by

$$\mathbf{y}_R = \begin{bmatrix} \Re(\mathbf{y}) \\ \Im(\mathbf{y}) \end{bmatrix}, \quad (44)$$

Algorithm 1 The EF-AA mechanism for iterative MIMO detections (BPSK modulation).

Input: the channel matrix \mathbf{H} estimated at receiver, the variance (power) of noise σ_n^2 , the maximum iteration number T for MIMO detections.

- 1: Initialize the counter for the iterative MIMO detection as $t = 1$.
- 2: **repeat**
- 3: **for** $l = 1$ to N_T **do**
- 4: **for** $i = 1$ to N_R **do**
- 5: Calculate the variance $var_{\omega_i^l}$ according to (35) and (36) at AIC, then transfer it to the EIC.
- 6: Update the mutual information $I_{\omega_i^l}$ as (10) at EIC.
- 7: Update the variance $var_{\psi_i^l}$ as (13) at EIC, then transfer it to the VN sub-detector.
- 8: Compute the mutual information $I_{\psi_i^l}$ based on (15) at the VN sub-detector.
- 9: **end for**
- 10: Calculate the mutual information I_{L_l} at the VN sub-detector according to (41).
- 11: **end for**
- 12: Calculate the averaged output mutual information I_L as (42).
- 13: Update counter for the iterative MIMO detection as $t = t + 1$.
- 14: **until** The maximum iteration number T is reached.

Output: The averaged output mutual information I_L of VNs in each iteration.

$$\mathbf{x}_R = \begin{bmatrix} \Re(\mathbf{x}) \\ \Im(\mathbf{x}) \end{bmatrix}, \quad (45)$$

and

$$\mathbf{n}_R = \begin{bmatrix} \Re(\mathbf{n}) \\ \Im(\mathbf{n}) \end{bmatrix}, \quad (46)$$

where each element corresponds to the information bit before QPSK modulation.

Therefore, through the aforementioned real-domain conversion, this paper extends the BPSK-modulated EF-AA mechanism to QPSK-modulated scenarios. In the following, the subscripts of matrix \mathbf{H}_R and vectors \mathbf{x}_R , \mathbf{y}_R , \mathbf{n}_R is omitted to better illustrate the derivation process.

Specifically, the complex QPSK symbol $x_l = \theta \in 1/\sqrt{2}\{1 + i, 1 - i, -1 + i, -1 - i\}$ can be transformed into the real form $x_l = \theta_R \in 1/\sqrt{2}\{1, -1\}$. Then the Gaussian approximation of the received symbol y_i is revised as

$$\begin{aligned} y_i &= \sum_{l=1}^{2N_T} h_{i,l}x_l + n_i \\ &= h_{i,l}x_l + \underbrace{\sum_{l'=1, l' \neq l}^{2N_T} h_{i,l'}x_{l'}}_{g_{il}} + n_i, \end{aligned} \quad (47)$$

correspondingly, the variance $\mathbb{V}(x_l)$ in the first iteration can be given as

$$\begin{aligned} \mathbb{V}(x_l) &= \frac{1}{2} \left[\left(\frac{1}{\sqrt{2}} \right)^2 + \left(\frac{-1}{\sqrt{2}} \right)^2 \right] - \left| \frac{1}{2} \left(\frac{1}{\sqrt{2}} - \frac{1}{\sqrt{2}} \right) \right|^2 \\ &= \frac{1}{2}. \end{aligned} \quad (48)$$

Under the QPSK modulation, the ECV $var_{\omega_i^l}$ defined in **Lemma 1** and variance $var_{\psi_i^l}$ in **Lemma 2** are computed as

$$var_{\omega_i^l} = \frac{2h_{i,l}^2}{\sigma_{g_{il}}^2}, \quad (49)$$

and

$$\text{var}_{\psi_i^l} = \sum_{i'=1, i' \neq i}^{2N_R} J^{-1} \left(I_{\omega_i^{i'}} \right), \quad (50)$$

respectively.

In addition, (28) and (29) in **Theorem 2** need to be modified as

$$\begin{aligned} P_i^l(+1/\sqrt{2}) &= P_i^l(\theta_j = +1/\sqrt{2}) \\ &= \begin{cases} \frac{1}{2} \left[1 + \text{erf} \left(\sqrt{\text{var}_{\psi_i^l}/8} \right) \right], & \text{if } x_l = +1/\sqrt{2}, \\ \frac{1}{2} \text{erfc} \left(\sqrt{\text{var}_{\psi_i^l}/8} \right), & \text{if } x_l = -1/\sqrt{2}, \end{cases} \end{aligned} \quad (51)$$

and

$$\begin{aligned} P_i^l(-1/\sqrt{2}) &= P_i^l(\theta_j = -1/\sqrt{2}) \\ &= \begin{cases} \frac{1}{2} \left[1 + \text{erf} \left(\sqrt{\text{var}_{\psi_i^l}/8} \right) \right], & \text{if } x_l = -1/\sqrt{2}, \\ \frac{1}{2} \text{erfc} \left(\sqrt{\text{var}_{\psi_i^l}/8} \right), & \text{if } x_l = +1/\sqrt{2}, \end{cases} \end{aligned} \quad (52)$$

Therefore, the ECV $\text{var}_{\omega_i^l}$ under the QPSK-modulated scenario can be calculated as in **Theorem 4**.

Theorem 4 Under the QPSK-modulated scenario, the ECV $\text{var}_{\omega_i^l}$ calculated at AIC is given as

$$\text{var}_{\omega_i^l} = \frac{4h_{i,l}^2}{\sum_{l'=1, l' \neq l}^{2N_T} |h_{i,l'}|^2 \left[1 + \text{erf} \left(\sqrt{\frac{\text{var}_{\psi_i^l}}{8}} \right) \right] \text{erfc} \left(\sqrt{\frac{\text{var}_{\psi_i^l}}{8}} \right) + 2\sigma_n^2}. \quad (53)$$

Proof: Similarly as in **Theorem 3**, under the QPSK modulation, the ECV $\text{var}_{\omega_i^l}$ in the subsequent iterations at AIC can be calculated depending on the following two cases:

CI: The transmit symbol $x_l = 1/\sqrt{2}$. With the probabilities $P_i^l(\mp 1/\sqrt{2})$ estimated at VN v_l shown as (51) and (52), the mean value $\mathbb{E}(x_l^+)$ and variance $\mathbb{V}(x_l^+)$ of x_l can be expressed as

$$\begin{aligned} \mathbb{E}(x_l^+) &= \frac{+1}{2\sqrt{2}} \left[1 + \text{erf} \left(\sqrt{\frac{\text{var}_{\psi_i^l}}{8}} \right) \right] - \frac{1}{2\sqrt{2}} \text{erfc} \left(\sqrt{\frac{\text{var}_{\psi_i^l}}{8}} \right) \\ &= \frac{1}{\sqrt{2}} \text{erf} \left(\sqrt{\frac{\text{var}_{\psi_i^l}}{8}} \right), \end{aligned} \quad (54)$$

and

$$\begin{aligned} \mathbb{V}(x_l^+) &= \left(\frac{1}{\sqrt{2}} \right)^2 P_i^l \left(\frac{1}{\sqrt{2}} \right) + \left(\frac{-1}{\sqrt{2}} \right)^2 P_i^l \left(\frac{-1}{\sqrt{2}} \right) - |\mathbb{E}(x_l)|^2 \\ &= \frac{1}{2} \left[P_i^l \left(\frac{-1}{\sqrt{2}} \right) + P_i^l \left(\frac{1}{\sqrt{2}} \right) \right] - \frac{1}{2} \left[\text{erf} \left(\sqrt{\frac{\text{var}_{\psi_i^l}}{8}} \right) \right]^2 \\ &= \frac{1}{2} \left[1 - \text{erf} \left(\sqrt{\frac{\text{var}_{\psi_i^l}}{8}} \right)^2 \right] \\ &= \frac{1}{2} \left[1 + \text{erf} \left(\sqrt{\frac{\text{var}_{\psi_i^l}}{8}} \right) \right] \text{erfc} \left(\sqrt{\frac{\text{var}_{\psi_i^l}}{8}} \right), \end{aligned} \quad (55)$$

respectively.

C2: The transmit symbol $x_l = -1/\sqrt{2}$. With the probabilities $P_i^l(\mp 1/\sqrt{2})$ estimated at VN v_l shown as (51) and (52), we can obtain the mean value $\mathbb{E}(x_l^-)$ and variance $\mathbb{V}(x_l^-)$ of x_l as

$$\begin{aligned}\mathbb{E}(x_l^-) &= \frac{-1}{2\sqrt{2}} \left[1 + \operatorname{erf} \left(\sqrt{\frac{\operatorname{var}_{\psi_i^l}}{8}} \right) \right] + \frac{1}{2\sqrt{2}} \operatorname{erfc} \left(\sqrt{\frac{\operatorname{var}_{\psi_i^l}}{8}} \right) \\ &= -\frac{1}{\sqrt{2}} \operatorname{erf} \left(\sqrt{\frac{\operatorname{var}_{\psi_i^l}}{8}} \right),\end{aligned}\quad (56)$$

and

$$\begin{aligned}\mathbb{V}(x_l^-) &= \frac{1}{2} - \frac{1}{2} \left[\operatorname{erf} \left(\sqrt{\frac{\operatorname{var}_{\psi_i^l}}{8}} \right) \right]^2 \\ &= \frac{1}{2} \left[1 + \operatorname{erf} \left(\sqrt{\frac{\operatorname{var}_{\psi_i^l}}{8}} \right) \right] \operatorname{erfc} \left(\sqrt{\frac{\operatorname{var}_{\psi_i^l}}{8}} \right),\end{aligned}\quad (57)$$

respectively.

It is obvious that under the QPSK modulation, the variance $\mathbb{V}(x_l)$ of x_l in subsequent iterations is irrelevant to the specific sign of x_l . Additionally, through initializing the variance of extrinsic LLR ψ_i^l as $\operatorname{var}_{\psi_i^l} = 0$, we can uniformly express the variance $\mathbb{V}(x_l)$ under different iterations as

$$\mathbb{V}(x_l) = \frac{1}{2} \left[1 + \operatorname{erf} \left(\sqrt{\frac{\operatorname{var}_{\psi_i^l}}{8}} \right) \right] \operatorname{erfc} \left(\sqrt{\frac{\operatorname{var}_{\psi_i^l}}{8}} \right). \quad (58)$$

Therefore, by substituting (58) into (35), the variance of LLR $\operatorname{var}_{\omega_i^l}$ can be presented by (53). \blacksquare

Referring to (50) and **Theorem 3**, the EF-AA mechanism under QPSK modulation is concluded in Algorithm 2.

Algorithm 2 The EF-AA mechanism for iterative MIMO detections (QPSK modulation).

Input: the channel matrix \mathbf{H} estimated at receiver, the variance (power) of noise σ_n^2 , the maximum iteration number T for MIMO detections.

- 1: Initialize the counter for the iterative MIMO detection as $t = 1$, and the variance $\operatorname{var}_{\psi_i^l} = 0$.
- 2: **repeat**
- 3: **for** $l = 1$ to $2N_T$ **do**
- 4: **for** $i = 1$ to $2N_R$ **do**
- 5: Calculate the variance $\operatorname{var}_{\omega_i^l}$ transferred from AIC to EIC according to (53).
- 6: Update the mutual information $I_{\omega_i^l}$ as (10).
- 7: Update the variance $\operatorname{var}_{\psi_i^l}$ transferred from EIC to the VN sub-detector based on (50).
- 8: Compute the mutual information $I_{\psi_i^l}$ as (15).
- 9: **end for**
- 10: Calculate the mutual information I_{L_l} as (41).
- 11: **end for**
- 12: Calculate the averaged output mutual information I_L as (42).
- 13: Counter updation $t = t + 1$.
- 14: **until** The maximum iteration number T is reached.

Output: The averaged output mutual information I_L of VNs in each iteration.

IV. NUMERICAL RESULTS

In this section, we utilize the proposed EF-AA mechanism to analyze the performance of FG-based iterative MIMO detections. Specifically, this section assesses the precision of the EF-AA mechanism from two aspects, i.e., the convergence under different iterations (by plotting AMI versus I_{ter} in Fig. 6) and the convergence under different received SNRs (by plotting AMI versus ρ_r in Fig. 9), respectively. More specifically, to verify the effectiveness of the proposed mutual information analysis method, the BER performance of the FG-based iterative MIMO detection under different iteration times and different received SNRs are presented in Fig. 7 and Fig. 10, respectively. In addition, the antennas at transmit and receive sides are equipped as $N_T = N_R = 4, 16$ for MIMO scenarios and $N_T = N_R = 128, 256$ for m-MIMO scenarios. In this section, the FG-BP iterative MIMO detection in [8] and QPSK modulation are adopted.

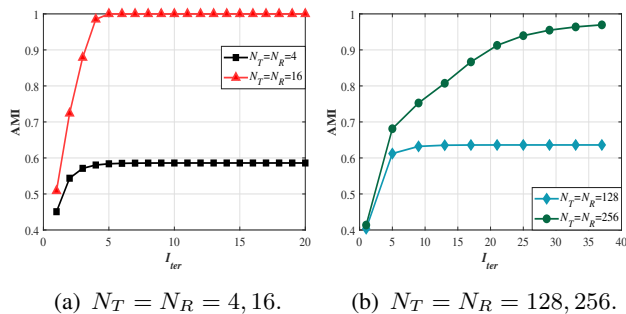


Fig. 6. The AMI of the FG-based iterative MIMO detection under different iteration times for various antenna equipment (where $\rho_r = 24$ dB and $\rho_r = 4$ dB from left to right).

Fig. 6 and Fig. 7 show that the proposed EF-AA mechanism can evaluate the convergence of FG-based iterative MIMO detections accurately. For example, Fig. 6(a) reveals that when the iteration number reaches 5, the AMI for both $N_T = N_R = 4$ and $N_T = N_R = 16$ approaches 1 identically. Moreover, the convergence performance of $N_T = N_R = 4$ and $N_T = N_R = 16$ in Fig. 6(a) are consistent with the BER performance in Fig. 7(a), which tend to be steady after 5th iteration. Likewise, Fig. 6(b) and Fig. 7(b) present identical convergence characteristics in AMI and BER performance.

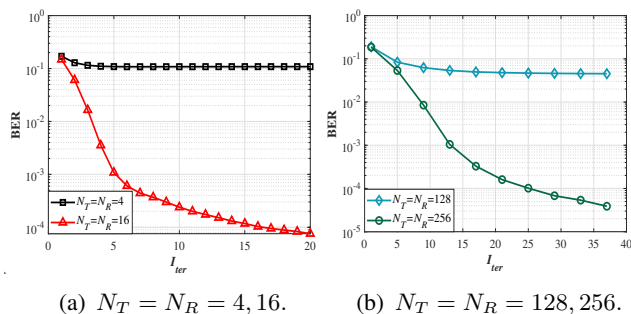


Fig. 7. The BER performance of the FG-based iterative MIMO detection [8] under different iteration times for various antenna equipment (where $\rho_r = 24$ dB and $\rho_r = 4$ dB from left to right).

Additionally, Fig. 8 is depicted to better demonstrate the evaluation accuracy of the proposed EF-AA mechanism on the convergence performance for the FG-based iterative MIMO detection. The left axis of Fig. 8 exhibits the BER performance, and the right axis displays the characteristic of AMI.

It can be seen from Fig. 8 that with the increase of iteration number I_{ter} , the decline of I_L (corresponding to AMI performance) and the growth of P_e curve (corresponding to BER performance) are exactly homologous. Specifically, both the I_L curve and P_e curve tend to keep stable after the 16th iteration.

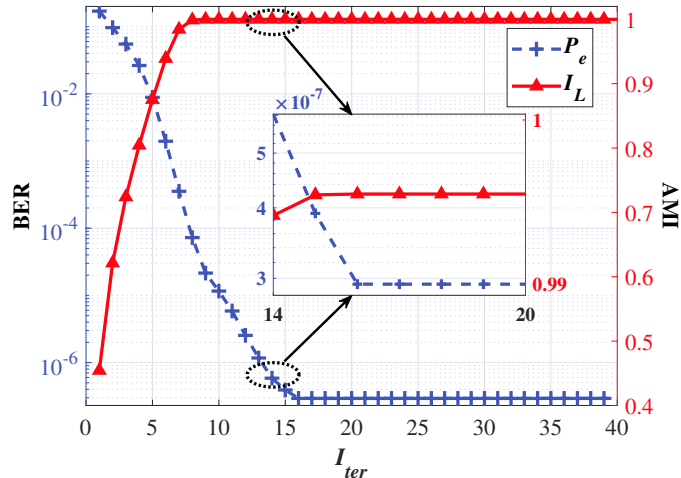


Fig. 8. The specific comparison between the EF-AA mechanism-calculated AMI and BER performance of [8] (where $\rho_r = 9$ dB).

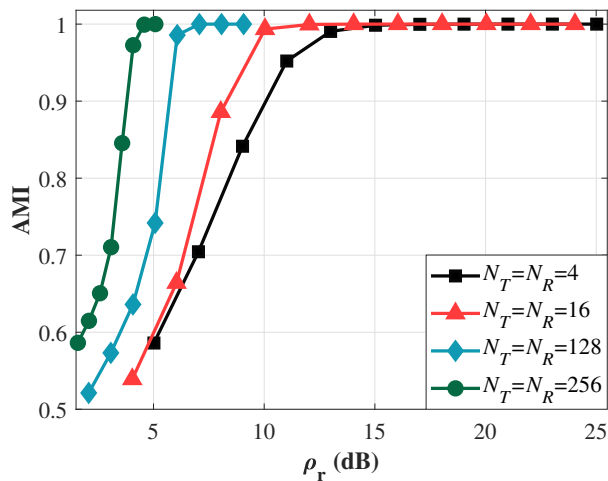


Fig. 9. The EF-AA mechanism calculated-AMI versus received SNR ρ_r of the FG-based iterative MIMO detection (where the maximum iteration number is $T = 40$).

Fig. 9 and Fig. 10 compare the AMI computed by the EF-AA mechanism and the BER performance of the FG-based iterative MIMO detection [8] under different antenna types of equipment. It can be seen that as the growth of antennas, the AMI curve (in Fig. 9) rises faster, and the BER curve (in Fig. 10) drops more dramatically. Additionally, Fig. 9 and Fig. 10 also exhibit the effectiveness of the proposed EF-AA mechanism. From Fig. 9, the convergence SNR under different antennas can be concluded as 4.5, 7, 14, 17 dB (from left to right) respectively. Then Fig. 10 shows that under antenna $N_T = N_R = 256, 128$, when the received SNR ρ_r reaches the convergence SNR in Fig. 9, the corresponding BERs tend to 0, which indicates the convergence of the FG-based iterative MIMO detection under m-MIMO scenarios. Then under antenna $N_T = N_R = 16, 4$, when the received SNR ρ_r reaches the convergence SNR in Fig. 9, the corresponding BERs tend to be steady, which indicates the convergence of the FG-based iterative MIMO detection.

V. CONCLUSIONS

This paper investigated the mutual information update flow of the FG-based iterative MIMO detection, particularly focusing on the convergence performance under different iteration numbers and SNRs. In this

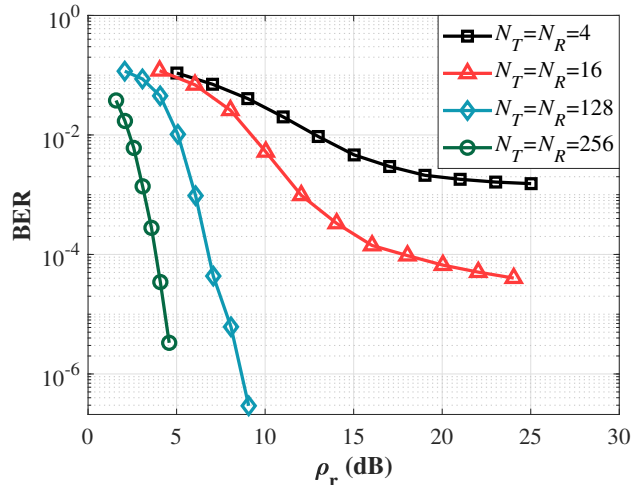


Fig. 10. The BER performance of the FG-based iterative MIMO detection [8] versus received SNR ρ_r (where the maximum iteration number is $T = 40$).

paper, the EF-AA mechanism was proposed to provide exact mutual information curves through Gaussian approximation and closed-form calculation under BPSK and QPSK modulations. Numerical results of AMI and BER performance demonstrate that for the MIMO and m-MIMO scenarios, the proposed EF-AA mechanism can evaluate the convergence characteristic of FG-based iterative MIMO detections in both precise iteration times and received SNRs. It can be foreseen that the proposed EF-AA mechanism might have significant impacts both on performance evaluation and algorithm optimization.

APPENDIX A CURVE FITTING FUNCTION $J(\cdot)$

As defined in [24], the mutual information I_γ between symbol s and LLR γ is given as

$$\begin{aligned}
 I_\gamma &= I(s; \gamma) \\
 &= \sum_{j=1}^q \int_{-\infty}^{\infty} p(s = \theta_j) p(\gamma | s = \theta_j) \log_2 \frac{p(\gamma | s = \theta_j)}{\sum_{j=1}^q p(\gamma, s = \theta_j)} d\gamma,
 \end{aligned} \tag{59}$$

where $p(s = \theta_j)$ denotes the *a priori* probability of the symbol s , $p(\gamma | s)$ denotes the conditional *a posteriori* probability of LLR γ , and $p(\gamma, s)$ denotes the joint *a posteriori* probability of LLR γ and symbol s .

Specifically, if the LLR γ follows the Gaussian distribution with mean of $\sigma^2/2$ and variance of σ^2 , then (59) can be expressed through the approximate curve fitting function $J(\cdot)$, which can be given as follows

$$J(\sigma) \approx \begin{cases} a_{J,1}\sigma^3 + b_{J,1}\sigma^2 + e_{J,1}\sigma, & 0 \leq \sigma \leq \sigma^*, \\ 1 - e^{(a_{J,2}\sigma^3 + b_{J,2}\sigma^2 + e_{J,2}\sigma + d_{J,2})}, & \sigma^* < \sigma < 10, \\ 1, & \sigma \geq 10, \end{cases} \tag{60}$$

in which

$$\begin{aligned}
 \sigma^* &= 1.6363, & a_{J,1} &= -0.0421061, & b_{J,1} &= 0.209252, \\
 e_{J,1} &= -0.00640081, & a_{J,2} &= 0.00181491, & b_{J,2} &= -0.142675, \\
 e_{J,2} &= -0.0822054, & d_{J,2} &= 0.0549608.
 \end{aligned} \tag{61}$$

Furthermore, the inverse function of $J(\cdot)$ is represented as

$$J^{-1}(I_\sigma) \approx \begin{cases} a_{\sigma,1}I_\sigma^2 + b_{\sigma,1}I_\sigma + e_{\sigma,1}\sqrt{I_\sigma}, & 0 \leq I_\sigma \leq I_\sigma^*, \\ -a_{\sigma,2} \ln [b_{\sigma,2}(1 - I_\sigma)] - e_{\sigma,2}I_\sigma, & I_\sigma^* < I_\sigma < 1, \end{cases} \tag{62}$$

where

$$\begin{aligned} I_\sigma^* &= 0.3646, & a_{\sigma,1} &= 1.09542, & b_{\sigma,1} &= 0.214217, \\ e_{\sigma,1} &= 2.33727, & a_{\sigma,2} &= 0.706692, & b_{\sigma,2} &= 0.386013, \\ e_{\sigma,2} &= -1.75017. \end{aligned} \quad (63)$$

APPENDIX B

DETAILED DERIVATION OF RIGHT AND WRONG DECISION PROBABILITIES

We show the details of the derivation of the equation of (33.b) and (34.b) in this appendix.

Firstly transform the first exponential term in equation (33.a) as $\frac{(\psi_i^l - \text{var}_{\psi_i^l}/2)^2}{2\text{var}_{\psi_i^l}} = t^2$, thus we have

$$t = \frac{(\text{var}_{\psi_i^l}/2 - \psi_i^l)}{\sqrt{2\text{var}_{\psi_i^l}}}, \text{ then we have}$$

$$\begin{aligned} & \frac{1}{2\sqrt{2\pi\text{var}_{\psi_i^l}}} \int_0^\infty \exp\left(-\frac{(\psi_i^l - \text{var}_{\psi_i^l}/2)^2}{2\text{var}_{\psi_i^l}}\right) d\psi_i^l \\ &= \frac{1}{2\sqrt{2\pi\text{var}_{\psi_i^l}}} \times \sqrt{2\text{var}_{\psi_i^l}} \int_{-\infty}^{\sqrt{\text{var}_{\psi_i^l}/8}} \exp(-t^2) dt \\ &= \frac{1}{4} \left(\frac{2}{\sqrt{\pi}} \int_0^{\sqrt{\text{var}_{\psi_i^l}/8}} \exp(-t^2) dt + \frac{2}{\sqrt{\pi}} \int_{-\infty}^0 \exp(-t^2) dt \right) \\ &\stackrel{(c)}{=} \frac{1}{4} \left(\frac{2}{\sqrt{\pi}} \int_0^{\sqrt{\text{var}_{\psi_i^l}/8}} \exp(-t^2) dt + \frac{2}{\sqrt{\pi}} \int_0^\infty \exp(-t^2) dt \right) \\ &= \frac{1}{4} \left[1 + \text{erf}\left(\sqrt{\frac{\text{var}_{\psi_i^l}}{8}}\right) \right], \end{aligned} \quad (64)$$

where $d\psi_i^l = -\sqrt{2\text{var}_{\psi_i^l}} dt$, and the sub-equation (64.c) holds because $\exp(-t^2)$ is an even function.

Similarly, the second term of equation (33.a) can be given as

$$\begin{aligned} & \frac{1}{2\sqrt{2\pi\text{var}_{\psi_i^l}}} \int_{-\infty}^0 \exp\left(-\frac{(\psi_i^l + \text{var}_{\psi_i^l}/2)^2}{2\text{var}_{\psi_i^l}}\right) d\psi_i^l \\ &= \frac{2}{4\sqrt{2\pi\text{var}_{\psi_i^l}}} \times \sqrt{2\text{var}_{\psi_i^l}} \int_{-\infty}^{\sqrt{\text{var}_{\psi_i^l}/8}} \exp(-t^2) dt \\ &= \frac{1}{4} \left[1 + \text{erf}\left(\sqrt{\frac{\text{var}_{\psi_i^l}}{8}}\right) \right], \end{aligned} \quad (65)$$

where $t = \frac{(\psi_i^l + \text{var}_{\psi_i^l}/2)}{\sqrt{2\text{var}_{\psi_i^l}}}$, and $d\psi_i^l = \sqrt{2\text{var}_{\psi_i^l}} dt$.

Follow the same principle of (64) and (65), we can deduct the terms of (34.a) as

$$\begin{aligned}
& \frac{1}{2\sqrt{2\pi var_{\psi_i^l}}} \int_0^\infty \exp\left(-\frac{(\psi_i^l + var_{\psi_i^l}/2)^2}{2var_{\psi_i^l}}\right) d\psi_i^l \\
&= \frac{2}{4\sqrt{\pi}} \int_{\sqrt{\frac{var_{\psi_i^l}}{8}}}^\infty \exp(-t^2) dt \\
&= \frac{1}{4} \operatorname{erfc}\left(\sqrt{\frac{var_{\psi_i^l}}{8}}\right),
\end{aligned} \tag{66}$$

with $t = \frac{(\psi_i^l + var_{\psi_i^l}/2)}{\sqrt{2var_{\psi_i^l}}}$, and

$$\begin{aligned}
& \frac{1}{2\sqrt{2\pi var_{\psi_i^l}}} \int_{-\infty}^0 \exp\left(-\frac{(\psi_i^l - var_{\psi_i^l}/2)^2}{2var_{\psi_i^l}}\right) d\psi_i^l \\
&= \frac{2}{4\sqrt{\pi}} \int_{-\infty}^{\sqrt{\frac{var_{\psi_i^l}}{8}}} \exp(-t^2) dt \\
&= \frac{1}{4} \operatorname{erfc}\left(\sqrt{\frac{var_{\psi_i^l}}{8}}\right),
\end{aligned} \tag{67}$$

with $t = \frac{(var_{\psi_i^l}/2 - \psi_i^l)}{\sqrt{2var_{\psi_i^l}}}$.

REFERENCES

- [1] W. Tong and P. Zhu, Eds., *6G: The Next Horizon: From Connected People and Things to Connected Intelligence*. Cambridge: Cambridge University Press, 2021.
- [2] D. Gesbert, M. Shafi, Da-shan Shiu, P. J. Smith and A. Naguib, "From theory to practice: an overview of MIMO space-time coded wireless systems," *IEEE J. Select. Areas Commun.*, vol. 21, no. 3, pp. 281-302, April 2003.
- [3] E. G. Larsson, O. Edfors, F. Tufvesson and T. L. Marzetta, "Massive MIMO for next generation wireless systems," *IEEE Commun. Mag.*, vol. 52, no. 2, pp. 186-195, February 2014.
- [4] Xu Zhu and R. D. Murch, "Performance analysis of maximum likelihood detection in a MIMO antenna system," *IEEE Trans. Commun.*, vol. 50, no. 2, pp. 187-191, February 2002.
- [5] D. Wubben, R. Bohnke, V. Kuhn and K. -D. Kammeyer, "Near-maximum-likelihood detection of MIMO systems using MMSE-based lattice- reduction," *2004 IEEE International Conference on Communications (IEEE Cat. No.04CH37577)*, Paris, France, 2004, pp. 798-802 Vol.2.
- [6] Huan Yao and G. W. Wornell, "Lattice-reduction-aided detectors for MIMO communication systems," *Global Telecommunications Conference, 2002. GLOBECOM '02. IEEE*, Taipei, Taiwan, 2002, pp. 424-428 vol.1.
- [7] F. R. Kschischang, B. J. Frey and H. -A. Loeliger, "Factor graphs and the sum-product algorithm," *IEEE Trans. Inf. Theory*, vol. 47, no. 2, pp. 498-519, February 2001.
- [8] S. Wu, L. Kuang, Z. Ni, J. Lu, D. Huang and Q. Guo, "Low-complexity iterative detection for large-scale multiuser MIMO-OFDM systems using approximate message passing," *IEEE J. Sel. Top. Signal Process.*, vol. 8, no. 5, pp. 902-915, October 2014.
- [9] X. Tan, Y. -L. Ueng, Z. Zhang, X. You and C. Zhang, "A low-complexity massive MIMO detection based on approximate expectation propagation," *IEEE Trans. Veh. Technol.*, vol. 68, no. 8, pp. 7260-7272, August 2019.
- [10] O. Oyman, R. U. Nabar, H. Bolcskei and A. J. Paulraj, "Characterizing the statistical properties of mutual information in MIMO channels," *IEEE Trans. Signal Process.*, vol. 51, no. 11, pp. 2784-2795, November 2003.
- [11] Zhengdao Wang and G. B. Giannakis, "Outage mutual information of space-time MIMO channels," *IEEE Trans. Inf. Theory*, vol. 50, no. 4, pp. 657-662, April 2004.
- [12] L. Musavian, M. R. Nakhai, M. Dohler and A. H. Aghvami, "Effect of channel uncertainty on the mutual information of MIMO fading channels," *IEEE Trans. Veh. Technol.*, vol. 56, no. 5, pp. 2798-2806, September 2007.
- [13] P. Yang, Q. Zou and H. Yang, "Message passing based calculation of MI and MMSE matrix for massive MIMO systems with finite-alphabet inputs," *IEEE Commun. Lett.*, vol. 25, no. 12, pp. 3824-3828, December 2021.

- [14] H. Gao, K. Xiao, B. Xia and Z. Chen, "Mutual information analysis of mixed-ADC MIMO systems over Rayleigh channels based on random matrix theory," *IEEE Trans. Wirel. Commun.*, vol. 19, no. 7, pp. 4894-4906, July 2020.
- [15] P. W. Wolniansky, G. J. Foschini, G. D. Golden and R. A. Valenzuela, "V-BLAST: an architecture for realizing very high data rates over the rich-scattering wireless channel," *1998 URSI International Symposium on Signals, Systems, and Electronics. Conference Proceedings (Cat. No.98EX167)*, Pisa, Italy, 1998, pp. 295-300.
- [16] S. Stiglmayr, J. Klotz and M. Bossert, "Mutual information of V-BLAST transmission," *2008 IEEE International Symposium on Wireless Communication Systems*, Reykjavik, Iceland, 2008, pp. 468-472.
- [17] F. Jiang, C. Li, Z. Gong and R. Su, "Extrinsic information analysis of a new iterative method using the stair matrix for massive MIMO uplink signal detection," *IEEE Wireless Commun. Lett.*, vol. 7, no. 6, pp. 1022-1025, December 2018.
- [18] T. Abiko et al., "An EXIT chart analysis for belief-propagation based detection in a large-scale MIMO system," *2013 IEEE 77th Vehicular Technology Conference (VTC Spring)*, Dresden, Germany, 2013, pp. 1-5.
- [19] H. Li, J. Guo, X. Wang, C. Cao and Z. Fei, "EXIT-aided scheduled iterative MIMO detection under non-homogeneous antenna propagation gain scenarios," *IEEE Trans. Veh. Technol.*, vol. 71, no. 10, pp. 10600-10614, October 2022.
- [20] Paul A. Samuelson, "A convergent iterative process," *J. Math. Phys.*, vol. 24, no. 1-4, pp. 131-134, April 1945.
- [21] Stephan ten Brink, "Convergence of Iterative Decoding," *Electronics Letters*, vol. 35, no.10, May 1999.
- [22] Andrews, Larry C, "Special functions of mathematics for engineers," British, *SPIE Optical Engineering Press*, 1998.
- [23] S. Yang and L. Hanzo, "Fifty years of MIMO detection: The road to large-scale MIMOs," *IEEE Commun. Surv. Tutor.*, vol. 17, no. 4, pp. 1941-1988, Fourthquarter 2015.
- [24] Thomas M. Cover and Joy A. Thomas, "Elements of information theory: Differential entropy," *John Wiley & Sons, Ltd*, pp. 243-259, 2005.